Performance analysis of IEEE 802.11n solutions combining MIMO architectures with iterative decoding and sub-optimal ML detection via MMSE and Zero forcing GIS solutions

M. K. Abdul Aziz, P.N. Fletcher and A.R. Nix
Centre for Communications Research, University of Bristol,
Merchant Venturers Building, Woodland Road,
Bristol, BS8 1UB, UK
E-mail: {M.K.Abdulaziz, Paul.Fletcher, Andy.Nix}@bristol.ac.uk

performance of two newly proposed IEEE 802.11n candidate solutions by suggesting extensions to 802.11a. The new solutions incorporate a MIMO architecture for the wireless links between the network terminals. The FEC block in the PHY layer chain is also enhanced with a Turbo encoder to provide interleaving gains for the larger sized PSDUs (1-4095 bytes). Due to the ambitious data rate targets identified in 802.11n, where 'on-air' data rates of up to 320Mbit/s are quoted, a large MIMO architecture comprising 6 Transmit and 6 Receive antenna elements is adopted. ML detection using such large configurations is often prohibitively complex due to an unrealistic enumerated symbol list. In this paper we propose Zero-Forcing and MMSE-GIS solutions to ease complexity at the receiver. PER results for these new schemes are presented and Link throughputs are compared to demonstrate the viability of the chosen solutions and their benefits over the existing 802.11a standard.

Keywords - 802.11a; 802.11n; MIMO; MMSE-GIS; ZF-GIS

I. INTRODUCTION

The commercial introduction of the IEEE 802.11b installation as a Wireless Local Area Network (WLAN) standard has been a tremendous success. This is partly due to its support for higher data rates, where up to 11Mbit/s is now commonplace. This favorable growth in the acceptance of WLAN technology is continuing with the addition of the 802.11a and 802.11g, the latter offering backwards compatibility to 802.11b. These new standard compatible solutions support peak nominal data rates of up to 54Mbit/s.

In recent years, advancements in the field of wireless communications have generated a great interest in the deployment of multiple element antenna arrays for mobile terminals. These methods have the potential to dramatically increase both performance and capacity [1]. The list for Multiple Input Multiple Output (MIMO) diversity enhancing techniques are well known and range from simple transmit delay diversity schemes to hand designed Space Time Trellis Coded (STTC) solutions [5] for optimal coding and diversity gains. Further combinatorial schemes that utilize MIMO architectures with Turbo decoding are also discussed in [3]. This is due to the exceptional performance shown by [4] provide an interleaving gain for superior performance with larger sized PSDUs. The channel coded bits are interleaved using the specified standard block interleaver before being assigned to their respective transmit antennas. The bits are finally mapped to symbol values according to the chosen 802.11a compatible modulation format. This architecture extends the use of Bit Interleaved Coded Modulation (BICM) [8] to MIMO architectures as the basis of its transmission strategy. At the receiving terminals, the signals are detected via a sub-optimal Maximum Likelihood (ML) solution in conjunction with Minimum Mean Squared Error (MMSE) and Zero Forcing Group Interference Suppressions (GIS). These methods are used to reduce the symbol enumerated search list. In this paper we refer to these schemes as MMSE-GIS and ZF-GIS solutions respectively. The calculated Log-Likelihood Ratio (LLR) observations are fed into an iterative decoder and a hard decision is made to retrieve the original binary information sent in the payload.

The paper is organized as follows. Section II elaborates on the PHY layer requirements to enable the proposed extension to IEEE 802.11a. This includes proposals in the FEC PHY chain and the use of MEAs at the mobile terminals. Section III explains the simulation setup, with section IV presenting PER results and section V giving the Link Throughput results. Finally, the paper concludes by comparing and discussing the performance of the MIMO architectures as a potential solution for 802.11n.

II. PHY LAYER REQUIREMENTS

The IEEE 802.11a standard FEC coding block comprises of a convolutional encoder that appends six zero tail bits before deploying puncturing via a mode independent P1 pattern [9]. This produces a code rate of 1/2 with 64 states for generator polynomials, $g_1=\{133_8\}$ and $g_2=\{171_8\}$. A corresponding mode dependent P2 pattern produces a further code rate of 3/4. Both of these patterns are presented in table 1. The IEEE 802.11a standard does not specify the type of decoder required, although this is commonly associated with either a hard or soft decision Viterbi decoder [10].

This research was sponsored by QinetiQ Ltd.

TABLE I. PUNCTURING PATTERN

Erased bits

S	S
P	P
P	P

Puncturing 1, 1/2-rate

S	S	S	S	S	S
P	P	P	P	P	P
P	P	P	P	P	P

Puncturing 2, 3/4-rate

It is proposed that the encoder be replaced by two parallel concatenated RSC encoders. The first encoder will be fed with the information bits, whereas the second encoder is fed with an interleaved version of the same bits. The interleaver is pseudorandom with a length specified by the number of bits in the Physical Layer Service Data Unit (PSDU) or payload. Terminating tail bits of ones and zeros are also appended to the PSDU bits to return the first RSC encoder to its zero state. This produces a natural mother code of rate 1/3; hence new mode dependent puncturing patterns are required to enable the different PHY modes. These new patterns are given in table 2.

TABLE II. PHY LAYER MODES

Mode	Modulation	Coding Rate, R_c	Bit Rate, $\Re$ [Mbit/s]	Extended Bit Rate, $\Re_{ext}$ [Mbit/s]
1	BPSK	1/2	6	36
2	BPSK	3/4	9	27
3	QPSK	1/2	12	72
4	QPSK	3/4	18	108
5	16QAM	1/2	24	144
6	16QAM	3/4	36	216
7*	64QAM	3/4	54	324

a.IEEE 802.11a optional mode

The FEC coded bits are fed through the standard block interleaver before undergoing serial-to-parallel multiplexing to assign each bit to its respective transmit antenna. The bits are grouped and converted to complex symbol values according to Gray coded constellation maps. The mapped symbols are arranged across defined data bearing subcarriers for an IFFT process that converts the frequency symbols into the time domain. A cyclic prefix of 800ns (25% of the useful symbol period) is appended to the end of each OFDM symbol. The proposed transmitter architecture is given in fig. 1.

In a MIMO architecture with m transmit antennas, a unique PHY burst is sent simultaneously from each antenna element. Therefore, a matrix of size m by M_c bits is required to construct the transmitted mapped symbols for each subcarrier, k, where M_c represents the number of bits per subcarrier. This is represented as shown in equation 1, where the Gray coded constellation mapping is imposed on the rows of $\boldsymbol{b_k}$. The number of information bits sent per OFDM symbol, I_{inf}, is given as indicated in equation 2, where R_c is the PHY mode code rate and N_{SD} is the total number of data bearing subcarriers (currently specified to be 48). See table 2 for a full description of the available PHY modes.

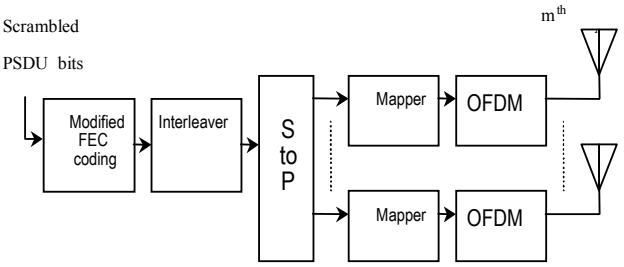

Figure 1: MIMO architecture applied to IEEE 802.11a Transceiver.

$$\boldsymbol{b_k} = \begin{bmatrix} b_{1,1} & b_{1,2} & \cdots & b_{1,M_c} \\ b_{2,1} & b_{2,2} & \cdots & b_{2,M_c} \\ \vdots & \vdots & \ddots & \vdots \\ b_{m,1} & b_{m,2} & \cdots & b_{m,M_c} \end{bmatrix} \quad (1)$$

$$I_{inf} = R_c M_c N_{SD} \quad (2)$$

The IEEE 802.11a standard allocates a bandwidth (including guard bands), B_W, of 20MHz and an OFDM symbol period (including guard interval), T_s, of 4µs. This results in a nominal bit rate that increases linearly with the number of transmit antennas deployed. This can be expressed mathematically by equation 3.

$$\Re_{ext} = m\left(\frac{I_{\inf}}{T_s}\right). \quad (3)$$

At the receiver the guard periods are removed and an FFT performed for the data received on each antenna element. The receiver architecture is shown in fig. 2.

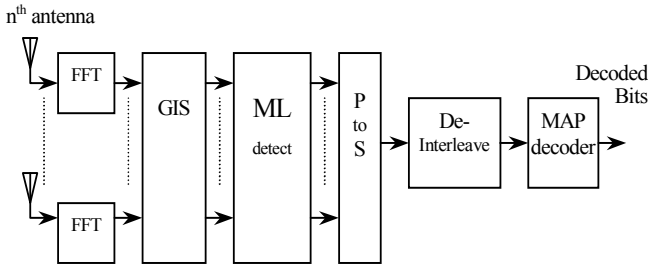

Figure 2. Proposed MIMO receiver architecture

III. ML DETECTION FOR GENERATION OF LLR

Since the FFT is a linear process, the extracted frequency domain data can be represented as summations of the transmitted symbols at a given subcarrier for all m transmit antennas. This is given as

$$R_{k,i} = \sum_{j=1}^{m} H_{k,i,j} C_{k,j} + \eta_{k,i}. \quad (4)$$

In a more compact form, (4) can be equivalently represented as

$$\boldsymbol{R_k} = \boldsymbol{H_k C_k} + \boldsymbol{\eta_k} \tag{5}$$

where

$$\boldsymbol{R_k} = [R_{k,1} \quad R_{k,2} \quad \cdots \quad R_{k,n}]^T \tag{6}$$

$$\boldsymbol{C_k} = map(\boldsymbol{b_k}) = [C_{k,1} \quad C_{k,2} \quad \cdots \quad C_{k,m}]^T \tag{7}$$

$$\boldsymbol{\eta_k} = [\eta_{k,1} \quad \eta_{k,2} \quad \cdots \quad \eta_{k,n}]^T \tag{8}$$

$$\boldsymbol{H_k} = \begin{bmatrix} H_{k,1,1} & H_{k,1,2} & \cdots & H_{k,1,m} \\ H_{k,2,1} & H_{k,2,2} & \cdots & H_{k,2,m} \\ \vdots & \vdots & \ddots & \vdots \\ H_{k,n,1} & H_{k,n,2} & \cdots & H_{k,n,m} \end{bmatrix} \tag{9}$$

with T denoting the matrix transpose and $H_{k,i,j}$ representing the channel values from transmit antenna j; $1 \le j \le m$ to receive antenna i; $1 \le i \le n$ for each of the data bearing subcarriers k; $-26 \le k \le 26$, $k \ne \{-21,-7,0,7,21\}$. $C_{k,j}$ represent the frequency domain mapped data symbols and $\eta_{k,i}$ are independent complex valued Gaussian noise samples of zero mean and variance per dimension σ^2.

Based on the received subcarriers, $\boldsymbol{R_k}$ and the Channel State Information (CSI) vector, which is obtained from the predefined SC-preamble for each corresponding subcarrier, the bit LLRs are computed by enumerating across all the possible mapped symbols for all transmit antennas. This follows the procedure in [11], where the generalized LLR (dropping subscript k) for any transmitted bit, $b_{p,q}$, where p; $1 \le p \le m$ and q; $1 \le q \le M_c$, is given as

$$\Lambda(b_{p,q}) = \log \frac{P[b_{p,q} = 1 \mid \boldsymbol{R}]}{P[b_{p,q} = 0 \mid \boldsymbol{R}]}. \tag{10}$$

Summing over all conditional probabilities (enumerated list of possible symbols) and taking into account the independence of the signals between receive antennas due to uncorrelated channel fades; we obtain bit level conditional probabilities given by equation (11), where each sent symbol bears the same probability of transmission and the received signals are corrupted by AWGN with a variance per dimension of σ^2. Equation (11) becomes the basis for our ML detector and for generation of LLRs prior to the iterative MAP decoder.

$$P[b_{p,q} \mid \boldsymbol{R}] = \sum_{\boldsymbol{C}:\boldsymbol{C}=map(\boldsymbol{b})} \prod_{i=1}^{n} \exp\left(- \frac{\left| R_i - \sum_{j=1}^{m} H_{i,j} C_j \right|^2}{2\sigma^2} \right) \tag{11}$$

IV. GIS SOLUTIONS

Due to the large MEA architectures proposed in this paper, the list of probable symbols sent for LLR calculation per binary bit become unrealistic for real time execution in hardware. In our configuration, where 6 independent PHY bursts are simultaneously transmitted across time and frequency, the deployment of the symbol mappings based on a 64QAM constellation would require a candidate list that is 6.8719×10^{10} long per sub-carrier for optimal ML detection.

Hence, as in [11], we propose to use the ZF-GIS and MMSE-GIS techniques to limit this enumeration list to be exponential in E_c rather than m, where E_c is referred to as the *enumeration constant*. A zero forcing solution is always possible in symmetric MIMO configurations with independent channel fades; however the process of grouping interferers will inevitably introduce rank deficient matrices. Therefore, there always exists a collection of *non*-unique vectors that result in the inner product result given by

$$\boldsymbol{W_{zf}}^H \boldsymbol{[} H_{des} \quad H_{\text{int}} \boldsymbol{]} = \boldsymbol{[} \hat{\boldsymbol{H}} \quad \boldsymbol{0} \boldsymbol{]} \tag{12}$$

where $\boldsymbol{W_{zf}}$ is the set of vectors that project the group of interferers, $\boldsymbol{H_{int}}$ into its *Nullspace* and ^{H} is the notation for a *Hermitian* transpose. The effects from the desired signal contributors form $\boldsymbol{H_{des}}$, the collection of columns that correspond to the particular transmitted symbols of interest such that the channel matrix is actually

$$\boldsymbol{H} = \boldsymbol{[} H_{des} \quad H_{\text{int}} \boldsymbol{]} \ . \tag{13}$$

Since the zero forcing solution is the set of vectors that exist in a subspace orthogonal to $\boldsymbol{H_{int}}$, these vectors can be found by reflecting itself upon $\boldsymbol{H_{des}}$. This is given as

$$\boldsymbol{W_{zf}} = \left\{ \left[\boldsymbol{I} - \overline{\boldsymbol{H}}_{\boldsymbol{int}} \left(\overline{\boldsymbol{H}}_{\boldsymbol{int}}^{\boldsymbol{H}} \overline{\boldsymbol{H}}_{\boldsymbol{int}} \right)^{-1} \overline{\boldsymbol{H}}_{\boldsymbol{int}}^{\boldsymbol{H}} \right] \boldsymbol{H_{des}} \right\} \tag{14}$$

where $\overline{\boldsymbol{H}}_{\boldsymbol{int}}$ is constructed by zeroing out columns occupied by $\boldsymbol{H_{des}}$ and a *Moore-Penrose* matrix inversion is applied. However since ZF-GIS suppressions fail to take into account noise statistics in its solution, the complete suppression of interferers run the risk of noise amplification.

$$\boldsymbol{W_{mmse}} = \left\{ \left[\left(\frac{\boldsymbol{P_T}}{\boldsymbol{m}} \right) \boldsymbol{H} \boldsymbol{H}^{\boldsymbol{H}} + \boldsymbol{\sigma}^{\boldsymbol{2}} \boldsymbol{I} \right]^{-1} \left(\frac{\boldsymbol{P_T}}{\boldsymbol{m}} \right) \boldsymbol{H} \overline{\boldsymbol{H}}_{\boldsymbol{des}}^{\boldsymbol{H}} \right\} \tag{15}$$

The MMSE-GIS offers a trade-off in the suppression of interferers and noise. Based on the *Wiener-Hopf* solution for minimization of error (a function of both noise and interferers), the MMSE-GIS tap weights are given as shown in equation 15. Here, $\overline{\boldsymbol{H}}_{\boldsymbol{des}}$ is constructed by zeroing out columns occupied by $\boldsymbol{H_{int}}$. Therefore, ignoring the suppressed interferers by applying the ZF-GIS or MMSE-GIS tap weights, generalized as $\boldsymbol{W}$, we obtain

$$\overline{\boldsymbol{R}} = \overline{\boldsymbol{H}}\boldsymbol{C} + \overline{\boldsymbol{\eta}} \tag{16}$$

where:

$$\overline{\boldsymbol{R}} = \boldsymbol{W}\boldsymbol{R} \tag{17}$$

$$\overline{\boldsymbol{H}} = \boldsymbol{W}\boldsymbol{H} \tag{18}$$

$$\overline{\boldsymbol{\eta}} = \boldsymbol{W}\boldsymbol{\eta} \tag{19}$$

Therefore, the GIS solutions for conditional bit probabilities as given by equation (11) become

$$P[b_{p,q} \mid \boldsymbol{R}] = \sum_{\boldsymbol{C}:\boldsymbol{C}=map(\boldsymbol{b})} \prod_{i} \exp\left(- \frac{\left| \overline{R}_i - \sum_{j} \overline{H}_{i,j} C_j \right|^2}{2\sigma^2} \right) \tag{20}$$

We observe that in the case of ZF-GIS, the values KE_c-E_c+1 $\leq i,j \leq KE_c$ are used, whereas for the MMSE-GIS, the values are KE_c-E_c+1 $\leq i \leq KE_c$ and 1 $\leq j \leq n$. K is the number of suppressions required in order to fully account for all the signals transmitted in each frequency slot occupied by an individual subcarrier. This reflects the reduction in the size of the candidate list for a more realistic ML solution.

V. Simulation Setup

The RSC encoders are described by [1, g_1/g_2], where the forward and feedback generator polynomials are given as $g_1=\{5_8\}$ and $g_2=\{7_8\}$ respectively, with 4 states. The payload for each PHY burst is 162 bytes long (with and without padded zero bits). These lengths enable an integer number of OFDM symbols to be sent per PHY burst at each transmitting antenna element. This corresponds to the IEEE 802.11a specification where the length field can be set between 1 and 4095 bytes in the PSDU. The receivers are sub-optimal ML detectors with ZF-GIS or MMSE-GIS solutions as presented in the previous section. Based on the assumption that the channel remains invariant throughout the MAC frame, calculation for the GIS filter tap weights are calculated for every individual data bearing subcarrier per GIS grouping. Here an enumeration constraint, E_c of 2 is used with K=3 being the number of GIS groupings to account for all 6 transmitted symbols.

The decoder employs a Maximum A-posteriori Probability (MAP) algorithm to realize an iterative decoding solution. Simulation results presented here are for hard decisions based on eight iterations of the BCJR implementation of this decoder [12]. The highest PHY mode 7, utilizing rate 3/4 with 64QAM, is not analyzed here since it is optional to the standard. A typical Non-Line-of-Sight (NLOS) indoor office environment (as specified by ETSI and IEEE) is assumed here for these simulations, which is widely known as channel A [13]. All results are based on PHY bursts sent over a statistically large set (1000-5000 independent realizations) of the channel model. The channel impulse response taps for the spatially separated terminals are subject to independent and uncorrelated Rayleigh fading. In the MIMO architecture, the overall transmit power is normalized to be equivalent to the 802.11a SISO case. Table 2 shows the PHY layer modes extended to the MIMO architecture used in this simulation.

VI. PER and Link Throughput Results

In this section, results are presented for the techniques discussed in section III of this paper. In particular, the proposed IEEE 802.11n solution based on ZF-GIS and MMSE-GIS solutions are analyzed. This is under the assumption that each packet uses CRC-r (Cyclic Redundancy Check) block codes for error detection. In the event of an erroneous packet or if a positive acknowledgment is not received, then the terminal will retransmit the packet [9]. Assuming that retransmission is deployed and the Link Adaptation scheme is ideally based on SNR, (ie, the mode with the highest throughput is chosen at any given SNR), the data throughput achieved is approximated as [14]

$$T_L = \Re_{ext}\,(1 - PER) \tag{21}$$

where $\Re_{ext}$ represents the link bit rate and PER denotes the Packet Error Rate for a specific PHY layer mode. MAC overheads are not accounted into approximation. The PER performance for the schemes are presented in figures 3 and 4 for ZF-GIS and MMSE-GIS solutions respectively.

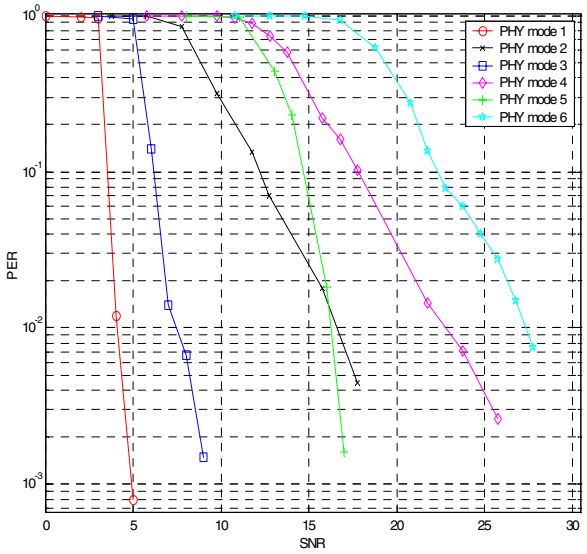

Figure 3: Proposed IEEE 802.11n PER for iteratively decoded payloads with MMSE-GIS solution of various PHY modes in ETSI channel 'A'.

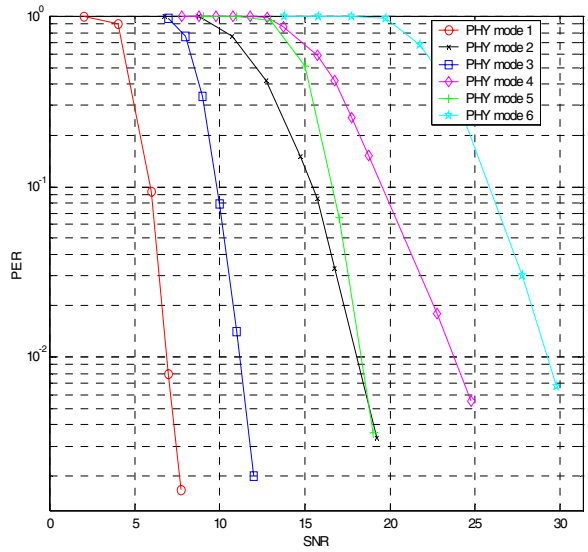

Figure 4: Proposed IEEE 802.11n PER for iteratively decoded payloads with ZF-GIS solution of various PHY modes over ETSI channel 'A'.

We can see that performance of the MMSE solutions are always superior, where at a PER of 1%, the average PER performance gain for PHY modes 1, 3 and 5 is 2.87dB whereas the average gain for PHY modes 2, 4 and 6 is 1.45dB. This makes a ZF-GIS solution more attractive for higher puncturing schemes (i.e. the second set of modes) as the expected gain from the MMSE-GIS decreases.

The Link Throughput performance results are presented in figures 5 and 6. We observe that at a SNR of 15dB, we are able to obtain Link Throughputs of 20.97 Mbit/s and 12 Mbit/s for MMSE-GIS and ZF-GIS respectively for our MIMO architecture. Link Throughputs in excess of 200 Mbit/s are achieved at 23dB and 27.5dB for the MMSE-GIS and ZF-GIS respectively. We also find that the Link Throughputs at any SNR offered by PHY modes 2 and 4 are always lower than PHY modes utilizing code rates of ½, due to their comparatively steep PER curves

A comparison of Link Throughput performance between the existing IEEE 802.11a standard and our proposed 802.11n solutions is given in table 3 for three different values of SNR (assuming ETSI channel A). Results for 802.11a Link Throughput have previously been presented in [15] and are repeated here for comparison. It can be seen that the MMSE-GIS 802.11n solution offers Link Throughput improvements (relative to ZF-GIS) of 17.8 Mbit/s, 53.8 Mbit/s and 47.5 Mbit/s at average SNR values of 5 dB, 15 dB and 25 dB respectively. Spatial multiplexing at these SNR values using the MMSE-GIS solution for a 6 transmit and 6 receive MIMO solution yields a throughput increase of 6.9, 5.6 and 4.3 times that of the equivalent 802.11a rate. Using the ZF-GIS solution, the improvement relative to 802.11a drops to 3.5, 3.2 and 3.3 times. Hence, at a low SNR of 5dB, the Link Throughput for the MMSE-GIS solution shows very promising results since it outperforms the expected Link Throughput increase of 6 independent data streams. This occurs because the Turbo decoder offer significant improvements over the standard Viterbi decoded packets in 802.11a at low SNRs.

TABLE III. COMPARISON OF 802.11A STANDARD AND 802.11N SOLUTION LINK THROUGHPUTS

WLAN standard/solutions	SNR (ETSI Channel A)		
	5 dB	15 dB	25 dB
IEEE 802.11a	5.2 Mbit/s	22.3 Mbit/s	48.4 Mbit/s
ZF-GIS 802.11n	18.1 Mbit/s	72.0 Mbit/s	160.4 Mbit/s
MMSE-GIS 802.11n	35.9 Mbit/s	125.8 Mbit/s	207.9 Mbit/s

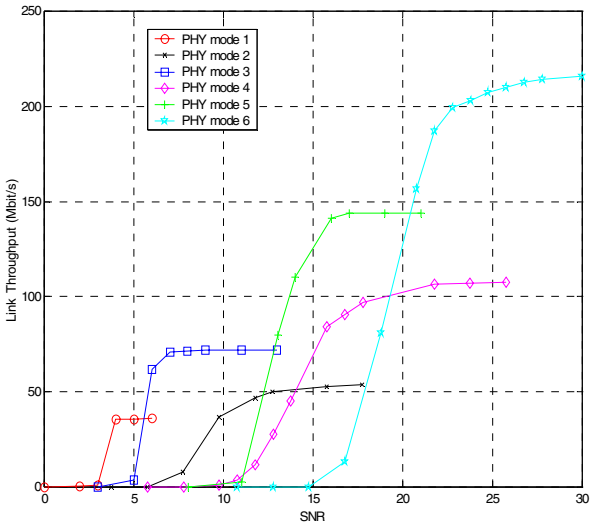

Figure 5: Link throughput versus SNR for proposed various 802.11n PHY modes based on the MMSE-GIS solution.

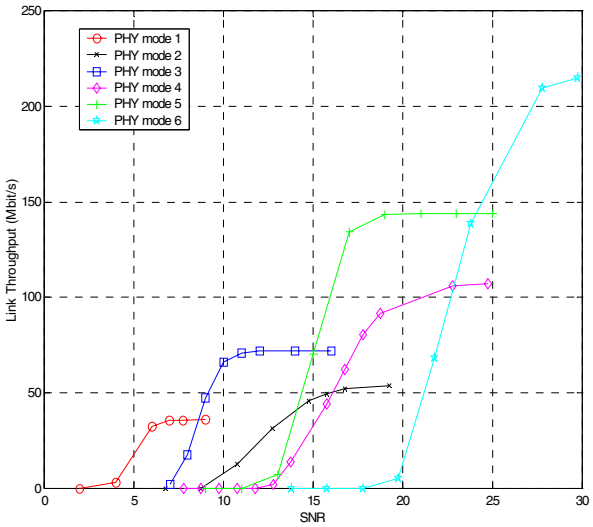

Figure 6: Link throughput versus SNR for proposed various 802.11n PHY modes based on the ZF-GIS solution.

VII. CONCLUSIONS

This paper has studied the application of multiple transmit and receive antennas for WLANs and proposed a new solution for IEEE 802.11n that is a logical extension of the existing 802.11a standard. The analysis was performed using the ETSI/IEEE specified indoor channel model (typical non-LOS office). PER and Link Throughput results were presented for two main receiver configurations and throughput results were compared with the existing 802.11a standard for a range of received SNR values.

It was shown that at low SNR, iterative turbo decoding in a NLOS indoor environment offers reliable performance, even when sub-optimal ML solutions are deployed. As expected, the detrimental effects of a low RMS delay spread channel, similar to slow fading in a narrowband Rayleigh channel, are removed when such large MIMO architectures are used to provide diversity in the system. Further performance improvement could be achieved by adopting a more rigorous PCCC encoder with a higher number of states, or by using a longer interleaver.

Although performance in terms of diversity increases, deploying a large numbers of transmit antennas poses a problem due to the increased computational overhead. This occurs because of the exponential growth in the number of possible symbols that could have been sent on each sub-band. This issue was resolved through the application of GIS based on Zero Forcing and MMSE criterions. In the ZF-GIS case, the loss of diversity and imperfect suppression due to noise amplification becomes a limiting factor for its performance. As a result, MMSE-GIS offers superior performance at all values of SNR and should be preferred to ZF-GIS as a GIS solution.

Assuming that time invariance is maintained throughout a MAC frame, the GIS tap filter weights can be calculated per individual subcarrier for each grouping. Hence each PHY burst would require 144 GIS solutions in addition to the reduced enumerated list for the sub-optimal ML solution.

In conclusion, results have shown that for the proposed IEEE 802.11n solutions, incorporating MIMO architectures with iterative decoding can significantly improve the level of expected Link Throughput. The deployment of a Turbo FEC system shows very good performance at low SNRs since the Link Throughput for an MMSE-GIS solution outperforms the given 6 independent data streams transmitted. However, further work needs to include an analytical investigation into the optimal value of E_c that trades off the loss in diversity with the reduction in complexity for specific case of MIMO-OFDM in an indoor channel. A more rigorous study of the MAC layer protocol should also be performed to achieve the ambitious system throughputs defined by the 802.11n High Throughput Working group.

ACKNOWLEDGMENTS

The authors wish to acknowledge the financial and technical support of QinetiQ Ltd. They also thank Dr. Angela Doufexi and Dr. Michael Butler for assisting and supporting the 802.11a simulations.

REFERENCES

[1] G.J. Foschini and M. Gans, 'On limits of wireless communications in a fading environment when using multiple antennas', Wireless Personal Communications, Vol. 6, pp. 311-335, 1998.

[2] V. Tarokh, N. Seshadri and A. Calderbank, 'Space-time codes for high data rate wireless communication - performance criterion and code construction', IEEE Trans. on Information Theory, Vol. 44, no. 2, pp. 744-765, March 1998.

[3] S. L. Ariyavisitakul, 'Turbo space-time processing to improve wireless channel capacity', IEEE Transactions on Communications, Vol. 48, pp. 1347–1359, Aug 2000.

[4] C. Berrou, A. Glavieux and P. Thitimajshima, 'Near Shannon limit error-correcting coding and decoding: Turbo codes', Proc. 1993 Int. Conf. Comm, pp 1064-1070, 1993.

[5] Y. Liu, P. Fitz and O. Takeshita, 'A full rate space-time turbo codes', IEEE JSAC, Vol. 19, no. 5, pp. 969-980, May 2001.

[6] D. Qiao, S. Choi, 'Goodput Enhancement in IEEE 802.11a Wireless LAN via Link Adaptation', Proc. IEEE ICC 2001, Helsinki, Finland, June 2001.

[7] IEEE Std 802.11: Wireless LAN Medium Access Control and Physical Layer Specifications, IEEE, Nov. 1997.

[8] G. Caire, G. Taricco and E. Biglieri, 'Bit-interleaved coded modulation', IEEE Trans. Inform. Theory, Vol. 44, pp 1121-1128, May 1999.

[9] IEEE Std 802.11a/D7.0-1999, Part11: Wireless LAN Medium Access Control (MAC) and Physical Layer (PHY) specifications: High Speed Physical Layer in the 5GHz Band, 1999.

[10] M. Butler and A. Nix, 'Quantization Loss for Convolutional Decoding in Rayleigh-fading Channels', IEEE Communications Letters, Vol. 7, Issue 9, pp. 446-448, Sep. 2003.

[11] A. Stefanov and T. Duman, 'Turbo-coded modulation for systems with transmit and receive antenna diversity over block fading channels: system model, decoding approaches, and practical considerations', IEEE JSAC, Vol. 48, pp. 1347-1359, Aug. 2000.

[12] W. E. Ryan, 'Concatenated Convolutional Codes and Iterative Decoding', to be published in the Wiley Encyclopedia of Telecommunications, http://www.ece.arizona.edu/~ryan, 2001.

[13] J. Medbo and P. Schramm, 'Channel Models for HIPERLAN/2', ETSI/BRAN document no. 3ERI085B, 1998.

[14] M.K. Abdul Aziz, P.N. Fletcher and A.R. Nix, 'Extension to the IEEE 802.11a standard incorporating iterative turbo decoding with transmit delay diversity', WPMC 2002, Oct. 2002.

[15] A. Doufexi, S. Armour, M. Butler, A. Nix and D. Bull, 'A Study of the Performance of HIPERLAN/2 and IEEE 802.11a Physical Layers', VTC Spring, May 2001.